ELSEVIER

Surface Science 372 (1997) 193–201

surface science

The adsorption site and orientation of CH_3S and sulfur on Ni(001) using angle-resolved X-ray photoelectron spectroscopy

D.R. Mullins [c], T. Tang [a], X. Chen [b], V. Shneerson [a], D.K. Saldin [b], W.T. Tysoe [a,*]

[a] *Department of Chemistry and Laboratory for Surface Studies, University of Wisconsin–Milwaukee, Milwaukee, WI 53211, USA*
[b] *Department of Physics and Laboratory for Surface Studies, University of Wisconsin–Milwaukee, Milwaukee, WI 53211, USA*
[c] *Oak Ridge National Laboratory, Oak Ridge, TN 37831-6201, USA*

Received 6 April 1996; accepted for publication 9 August 1996

Abstract

Photoelectron diffraction from the S 2p core level has been used to determine the adsorption site and orientation of sulfur and methyl thiolate (CH_3S) on Ni(001) by comparing the experimental data with the results of multiple scattering calculations. The theory was initially checked for atomic S, which is known to adsorb in the four-fold hollow site on Ni(001), and the results corresponded to the correct geometry. Comparison of calculated spectra with the experimental data indicates that chemisorbed atomic sulfur is located at 1.30 ± 0.01 Å above the first layer of nickel atoms on the (001) plane. At 100 K, CH_3S adsorbs in the four-fold site on Ni(001), where the C–S bond is proposed to be oriented along the surface normal on Ni(001). A comparison between calculated and experimental results demonstrate that the C–S bond in adsorbed methyl thiolate is oriented perpendicular to the surface and is 1.85 ± 0.1 Å long.

Keywords: Chemisorption; Computer simulations; Low index single crystal surfaces; Nickel; Photoelectron diffraction; Soft X-ray photoelectron spectroscopy; Thiols

1. Introduction

The formation of methyl thiolate, CH_3S, is the well-established first step in the thermal decomposition of methanethiol, CH_3SH, on most metal surfaces [1–10]. Several chemically distinct states of sulfur have been identified from the S 2p core-level photoemission peaks following CH_3S adsorption, leading to the conclusion that these different S 2p signals arise from different CH_3S adsorption states.

A trend has been observed in the S 2p binding energies for atomic S adsorbed on different metals. In general, the S 2p binding energy decreases as the coordination of the adsorption site decreases. On W(001), the S 2p binding energy decreases with increasing sulfur coverage [11]. This effect has been ascribed to a change in sulfur adsorption site from a four-fold site to a three-fold site due to a surface reconstruction [12]. On Ni(111) the same trend is found. Large sulfur coverages cause a surface reconstruction that changes the sulfur adsorption site from a three-fold to a four-fold site, which causes an increase in the S 2p binding energy [13]. In these cases, a variety of structural probes have been used to verify the sulfur adsorption site

* Corresponding author. Fax: +1 414 229 5530; e-mail: wtt@alpha2.csd.uwm.edu

PII S0039-6028(96)01099-0

and thereby establish the relationship between adsorption site and binding energy.

This relationship between S 2p peak position and coordination of the adsorption site has been applied in interpreting the S 2p spectra of CH_3S on different surfaces. Two chemically distinct thiolate intermediates have been observed upon adsorption at 100 K on W(001) [7] and Ru(0001) [8]. The highest binding-energy species was ascribed to a thiolate adsorbed in the highest-coordination adsorption site available, i.e. the four-fold site on W(001) and a three-fold site on Ru(0001). The lower binding-energy states were then assigned to a lower coordination site, either bridge or atop sites. No direct structural probes were used to confirm these assignments, however.

A comparison between the S 2p binding energy for atomic S and CH_3S on Ni(001) suggests that the CH_3S is adsorbed in a four-fold site. In this paper we will firmly establish the adsorption geometry of CH_3S on Ni(001) by comparing the experimentally measured photoelectron angular distributions with theoretically calculated distributions for various model structures. A priori knowledge of the nature of the sulfur adsorption site was extremely important in restricting the number of test geometries, which therefore allows the correct structure to be determined using as small a set of geometries as possible. The key to success for this strategy is to have effective methods for calculating accurately the structure of the adsorbed species from the angular distribution of photoemitted electrons. This is done using the method of Saldin et al. [14], which takes advantage of the local nature of the scattering process by constructing an environment around the scattering center (in this case the sulfur atom) from concentric shells that are almost equidistant from the center [15]. The radius of the largest shell required for the calculation is established just from the mean free path of the electron at the kinetic energy of the outgoing wave. This protocol will be discussed in greater detail below. In order to establish the accuracy of the method, we have first calculated the geometry of sulfur adsorbed on Ni(001), which has been measured using a number of other techniques. The strategy is then applied to examining the geometry of the adsorbed thiolate.

2. Experimental

The Ni(001) sample was aligned by Laué back-reflection and mechanically polished. The sample was cleaned using repeated cycles of Ar-ion sputtering followed by annealing to 1000 K until no surface contaminants were detected using Auger electron spectroscopy (AES). Although the Auger spectrum indicated that the sample was clean, the C 1s photoelectron spectrum indicated the presence of a persistent atomic C coverage of ~ 0.05 ML, possibly due to subsurface carbon. The clean Ni(001) sample produced a clear $p(1 \times 1)$ LEED pattern with low background intensity. The breadth of the LEED spots suggested that there may have been relatively narrow terrace widths.

Atomic S was deposited using H_2S dosed at 300 K, and then the sample was annealed to 1000 K. Methanethiol was dosed at a sample temperature of 100 K and then the sample was annealed to 150 K to desorb physisorbed thiol.

Photoemission spectra were recorded using a VSW EA125 hemispherical analyzer. The acceptance angle was $\pm 2°$, based on the manufacturer's specifications. Normal emission was established by sighting the back-reflection from the sample through a viewport in the analyzer and was accurate to within $\pm 2°$. The sample was oriented as shown in Fig. 1. The emission plane was normal to the surface and contained the [100] azimuth. Excitation radiation was obtained from beamline U13UA at the National Synchrotron Light Source. The incident radiation was in the emission plane and the angle between the incident radiation and the emission direction was fixed at 65°. Angle-dependent X-ray photoelectron diffraction (XPD) data were collected by rotating the sample. The excitation energy was selected in order to produce the desired photoelectron kinetic energy.

3. Calculation of angle-resolved photoemission data

As is the case with low-energy electrons employed in other surface-structure probes, photoelectrons scatter strongly from atoms within the sample. Consequently, the accurate simulation of

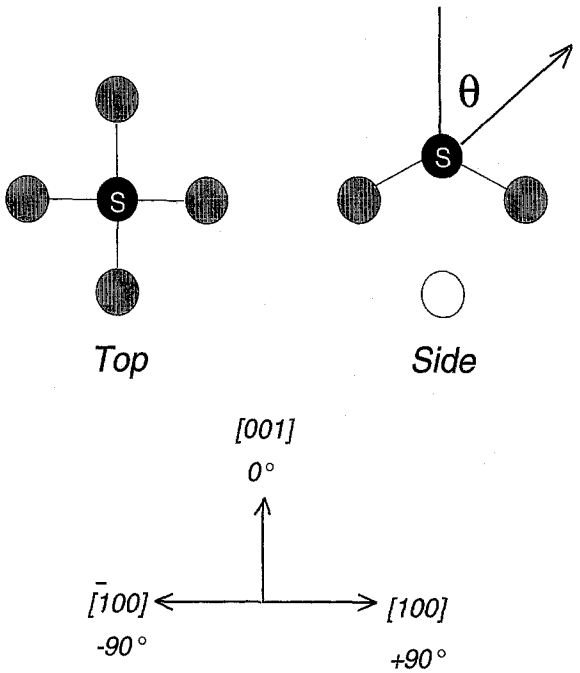

Fig. 1. Experimental geometry for studying the angular dependence of S 2p emission on Ni(001). Second-layer Ni is shown in white, first-layer Ni in gray, and S in black. The emission plane contains the [001] and [100] azimuths for Ni(001). Indicated also is the polar angle θ.

photoelectron diffraction patterns is a challenging exercise in multiple-scattering theory. Unlike the case of low-energy electron diffraction (LEED), where the probe electrons form a broad wavefront incident on a sample from the outside, core-level photoelectrons are generated from individual atoms within a sample. The point nature of such electron sources suggests that an advantageous computational strategy might be to exploit the short elastic mean-free path of the photoelectrons to restrict considerations of their scattering to a local cluster of atoms centered on the photoemitter. This strategy forms the basis of the concentric-shell algorithm of Saldin et al. [14]. In that scheme, the calculations are rendered tractable by the division of the cluster into a series of concentric shells centered on the photoemitter. The resulting division of the multiple scattering into intra- and inter-shell portions results in significant savings of computer time, as in analogous calculations of X-ray absorption near-edge structure (XANES) [16] for instance, while not sacrificing accuracy.

4. Results

4.1. Photoemission

The S 2p photoelectron spectrum from S on Ni(001) is shown in Fig. 2A. The photon energy was 250 eV, giving a photoelectron kinetic energy (KE) of 80–90 eV, and the emission angle was 15°. The S $2p_{3/2}$ binding energy is 161.55 eV. The S 2p spectrum from CH_3S on Ni(001) is displayed in Fig. 2B. CH_3S led to two chemically distinct sulfur states on Ni(001) at 150 K. The dominant state has a S $2p_{3/2}$ binding energy of 163.35 eV, with a much weaker state appearing at 162.00 eV. Both are attributed to CH_3S. The species at lower binding energy is attributed to CH_3S adsorbed at step edges. When the sample is annealed, both of these

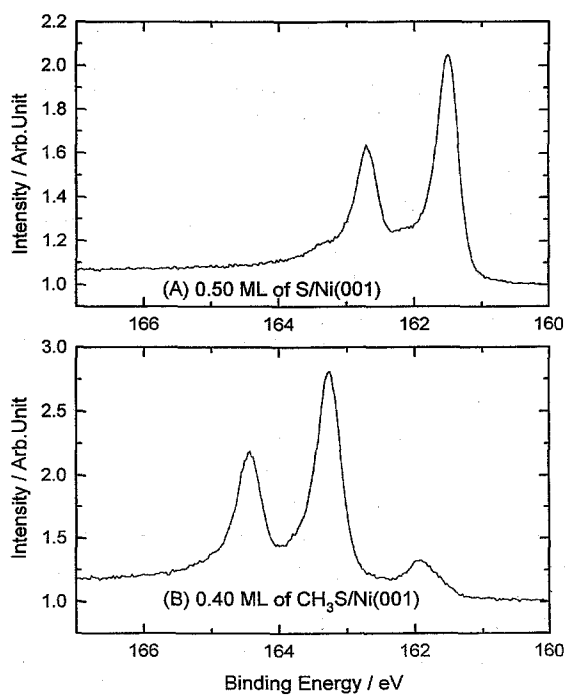

Fig. 2. (A) S 2p photoemission spectra for 0.50 ML of S and (B) from a saturation coverage of CH_3S at 150 K on Ni(001). The photon energy was 250 eV.

states disappear and atomic S forms, yielding a 2p binding energy of 161.70 eV.

The C 1s spectra (not shown) reveal a single peak at 284.6 eV at 150 K. When the sample is annealed, the total C 1s intensity decreases due to CH_4 desorption and the resulting atomic carbon exhibited a new peak at 283.8 eV [9].

4.2. X-ray photoelectron diffraction

Several factors were taken into account in order to determine reliably the relative intensities of the S 2p photoemission peaks at different emission angles. During the course of the experiment the current in the storage ring decays, causing a reduction in the incident flux. It was found that the most reproducible method for normalizing to the incident flux was to divide the peak intensity by the background intensity at several eV higher kinetic energy. In addition, as the sample is rotated, the incident and emission angles change simultaneously, causing the intensity to vary for geometrical/instrumental reasons.

The instrumental angular variation was determined in two ways. First, the S 2p spectra from atomic S on Ni(111) was recorded as a function of emission angle using Mg Kα excitation (1263 eV). The resulting photoelectrons had a kinetic energy of about 1100 eV. At this kinetic energy, forward scattering predominates [17] and since sulfur is present as an overlayer, no diffraction occurs. The normalized S 2p intensity using Mg Kα excitation for S on Ni(111) is shown in Fig. 3A. The angular dependence shows a minimum at normal emission and then increases smoothly with increasing emission angle until the signal diminishes rapidly at higher angles. This method does not provide an ideal determination of the instrument function because the sources (anode versus synchrotron beamline) had a different incident geometries. In addition, there were small differences in sample position in the laboratory and at the synchrotron that affected the cut-off angle. The variation in the background intensity with emission angle is also different at 1100 eV compared to that at the lower kinetic energies used in the XPD experiments. An alternative method is demonstrated in Fig. 3B. Fernández et al. [18] have shown that the methyl

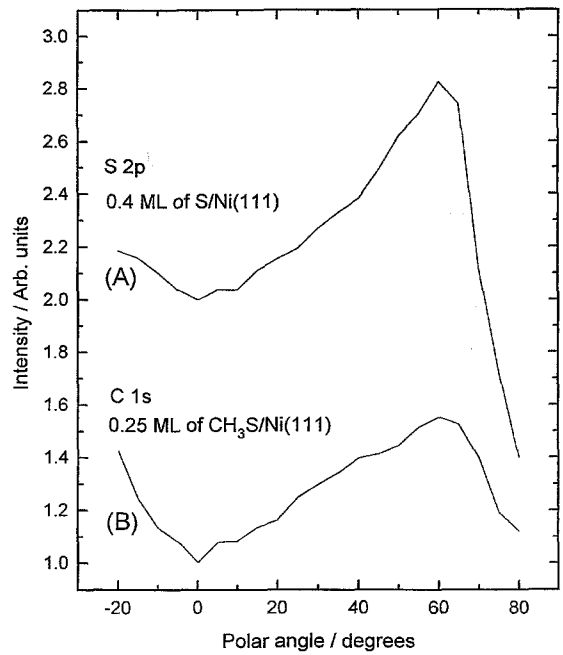

Fig. 3. (A) Angular dependence of the S 2p signal from 0.4 ML of atomic S on Ni(111) excited using Mg Kα (1263 eV) giving a photoelectron kinetic energy of ~1100 eV. (B) Angular dependence of the C 1s intensity from 0.25 ML of CH_3S on Ni(111) annealed to 150 K excited using ~485 eV photons giving a photoelectron kinetic energy of ~200 eV.

group in CH_3S on Ni(111) at 100 K is tilted toward the surface. Assuming that the orientation is also azimuthally averaged, the C 1s photoemission is not expected to show any angular anisotropy. Fig. 3B shows the C 1s angular variation from CH_3S on Ni(111) at 100 K at 200 eV kinetic energy. The shape of this curve is very similar to Fig. 3A, with no sharp features at any angle. This curve was used to represent the instrument function because it was obtained under identical experimental conditions as the S 2p data on Ni(001).

Diffraction results from an atomic overlayer of sulfur on Ni(001) (with a binding energy of 161.55 eV) are shown in Fig. 4A. The S 2p kinetic energy was nominally 200 eV and the data have been scaled so that the minimum between −20 and 60° is equal to 1. The angular variation in intensity exhibits two peaks at large off-normal angles of 40 and 55°. In addition, there is a sharp peak evident at normal emission.

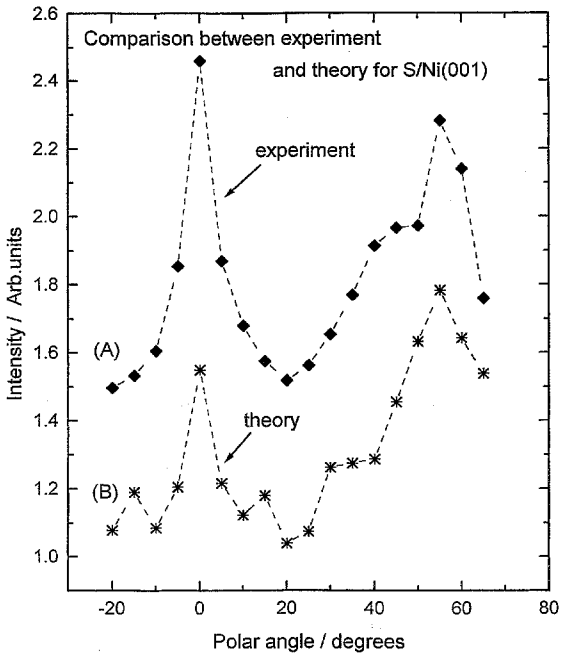

Fig. 4. (A) Sulfur 2p angular dependence at 200 eV kinetic energy for 0.45 ML S on Ni(001). (B) Calculated S 2p angular dependence for S adsorbed in a four-fold site, 1.30 Å above the first Ni layer.

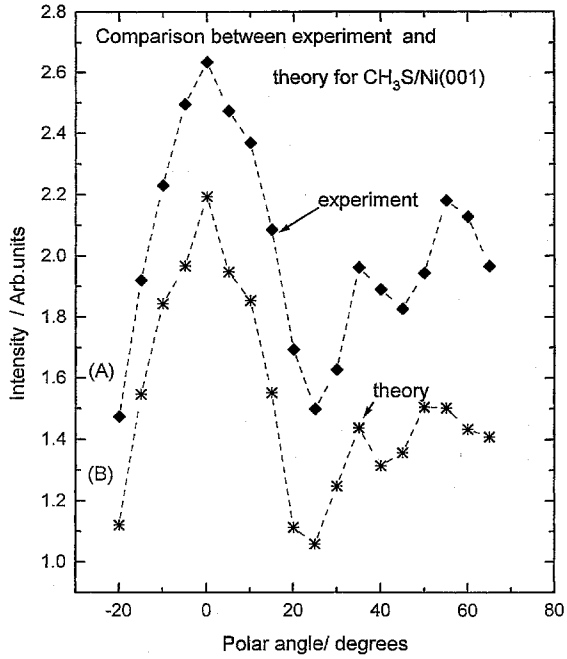

Fig. 5. (A) Sulfur 2p angular dependence at 200 eV kinetic energy for 0.30 ML CH_3S adsorbed on Ni(001) annealed to 150 K. (B) Calculated S 2p angular dependence for CH_3S adsorbed in a four-fold site, 1.30 Å above the first Ni layer and the C–S bond normal to the surface (1.85 Å long).

Diffraction data for the S 2p signal at 200 eV KE from CH_3S on Ni(001) are shown in Fig. 5A. Again, two peaks are seen at 35 and 55°, as well as an intense and broad feature at normal emission.

5. Discussion

The X-ray photoelectron diffraction results for atomic S on Ni(001) provide a benchmark for interpreting the data for CH_3S. Sulfur adsorbs in the four-fold hollow site on Ni(001) at a height of 1.30 Å above the top Ni layer [19–22]. There is a Ni atom directly beneath the S atom in the second layer. This geometry can be used to interpret the XPD data shown in Fig. 4A. Since the sulfur is adsorbed as an overlayer, none of the peaks can be attributed to forward scattering and, to a first approximation, the peaks can be assigned to back-scattering along the S–Ni bond directions. Backscattering is therefore expected at normal emission from the Ni atom in the second layer and near 55° from the first-layer Ni atom along the [100] azimuth (see Fig. 1).

The angle-resolved data were calculated for sulfur adsorbed at the center of the four-fold hollow site on Ni(001). The substrate geometry was taken to be that of a truncated single crystal of nickel and the vertical sulfur–nickel distance was varied between 1.25 and 1.4 Å. The correspondence between the experimental and theoretical result was calculated from a D factor:

$$D(\alpha,\beta)=\frac{\sqrt{\sum_i (\alpha+\beta E_i-C_i)^2}}{\sum_i E_i},$$

where E_i are the experimental data and C_i the corresponding calculated results. β and α represent a scaling factor and an offset correction, respectively, between the experimental and calculated data, and D is minimized with respect to α and β for each trial geometry to obtain the best compari-

son between the experimental data and the calculated angular distribution. The variation in D is shown plotted in Fig. 6 for sulfur on Ni(001) as a function of the distance of the sulfur atom to the Ni(001) surface. Clearly D is rather sensitive to the geometry and the minimum in this value corresponds to a vertical S–Ni distance of ~ 1.30 Å. The error in this value σ_R is estimated from $\sigma_R = (dR/dD)\sigma_D$, where (dR/dD) is obtained from the slope of the D factor versus geometrical parameter (in this case the S–Ni distance) adjacent to the minimum. The value σ_D represents an estimate of the statistical error in the D-factor displayed above. If the total number of electrons counted to collect the ith measurement in the angular distribution is n_i, then the statistical error in this measurement is $\sqrt{n_i}$. This yields a value of σ_D by substitution into the above equation as

$$\sigma_D = \frac{\sqrt{\sum_i n_i}}{\sum_i n_i},$$

which varies approximately as $1/\sqrt{n_i}$. A conservative estimate for the total number of electrons counted at each point is $\sim 10^6$ giving a corresponding value of σ_D of 10^{-3}. This gives the vertical S–Ni distance as 1.30 ± 0.01 Å, leading to a S–Ni bond distance of 2.20 ± 0.02 Å, and is in good agreement with measurements on both Ni(111) and Ni(001) using other methods [19–22]. The best-fit spectrum (for a vertical S–Ni distance of 1.30 Å) is shown in Fig. 4B, and clearly the agreement between theory and experiment is good.

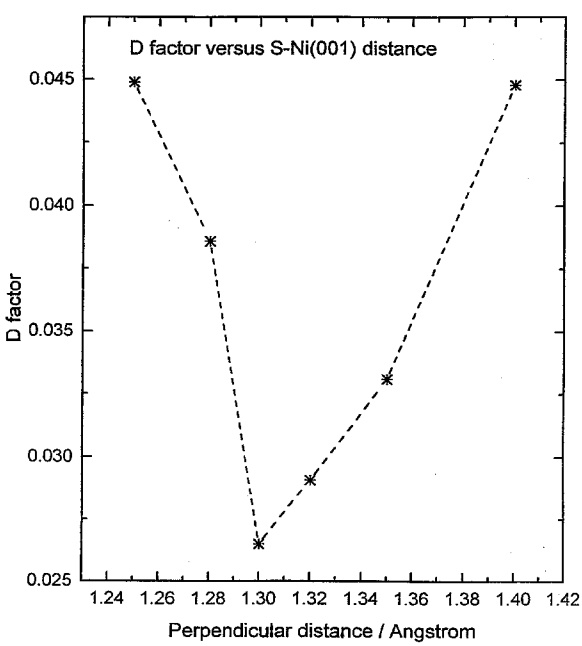

Fig. 6. Plot of the quality of fit parameter D (see text) versus the vertical S–Ni distance for the photoelectron angular distribution of S/Ni(001).

As shown in Fig. 1, as the Ni(001) sample is rotated toward positive angles, the Ni atom in the first layer that lies in the [100] direction becomes aligned behind the S atom along the analyzer axis. This results in a bond angle of about 55° with respect to the surface normal, and is consistent with the peak maximum at 55° in Fig. 4. In addition, S on Ni(001) has a peak at normal emission because the second-layer Ni atom is aligned behind the S atom in this direction. The origin of the additional peak at 40° on Ni(001) is uncertain.

The XPD results for CH_3S at 100 K on Ni(001) are qualitatively similar to the results obtained for *atomic* sulfur on this surface (compare Figs. 4 and 5). In particular there is a doublet between 35 and 55° in both sets of data. There is also a broad peak evident at 0°. Since the features at large scattering angles are similar to those for sulfur adsorbed on Ni(001), this suggests that the sulfur adsorption site is the same for the thiolate species as for atomic sulfur. In addition, the S 2p binding energy is 1.8 eV greater for CH_3S than for S in the four-fold site. This shift to higher binding energy is primarily due to the S being in a molecular species. However, if the coordination of the adsorption site for CH_3S was less than the atomic S, the binding energy would be reduced, and possibly even be smaller than the atomic S binding energy. This occurs on W(001), where two thiolates were observed. One thiolate had a binding energy greater than the atomic S binding energy, while the other thiolate's binding energy was smaller than the atomic S binding energy [7]. A qualitative interpretation of the data therefore places thiolate species in the four-fold hollow site.

In order to confirm the CH_3S adsorption site, the angular distribution was calculated for a thiolate species adsorbed in the bridge, four-fold, and

atop sites on Ni(001). In all cases, the S–Ni bond length was taken to be 2.20 Å and the C–S bond length 1.85 Å. The values of the S–Ni and C–S bond lengths used in these simulations are close to those found for atomic S on Ni [19–22] and for gas-phase CH_3SH [23], respectively. The C–S bond was oriented normal to the surface (see below). The results are displayed in Fig. 7, which compares calculated angular distributions for a thiolate species adsorbed on four-fold site (Fig. 7A), an atop site (Fig. 7B) and a bridge site (Fig. 7C), with the experimental data. Clearly, the agreement between the experimental results and the calculations for the atop and bridge sites is significantly worse than the agreement for the thiolate adsorbed in the four-fold site. The differences between the experimental data and the calculated angle-resolved data for the atop and bridge sites is sufficiently large that slight changes in the bond lengths will not lead to agreement.

The significant enhancement at normal emission in the presence of a surface thiolate also implies that the C–S axis is oriented perpendicular to the surface. In order to test this, the D factor was calculated, again using a S–Ni bond length of 2.20 Å and a S–C bond length of 1.85 Å as a function of the tilt angle from the normal along the [110] and the [100] azimuths. The resulting data are plotted in Fig. 8, which reveal a minimum at $0 \pm 10°$ for both directions, indicating a C–S bond oriented normal to the surface. The error was calculated using the method described above.

Finally, the angle-resolved intensity was calculated as function of the C–S bond length for values between 1.75 and 2.0 Å and for various vertical S–Ni distances between 1.25 and 1.35 Å, and the D factor was determined as described above. The minimum value of D as a function of the vertical S–Ni distance is plotted for a C–S distance of 1.85 Å in Fig. 9. The minimum in this curve is at a vertical S–Ni distance of 1.30 ± 0.03 Å, indicating that the S–Ni distance is identical for atomic S and for methyl thiolate. The D value is plotted as a function of C–S distance for a fixed S–Ni distance of 2.20 Å in Fig. 10. This curve is rather shallow,

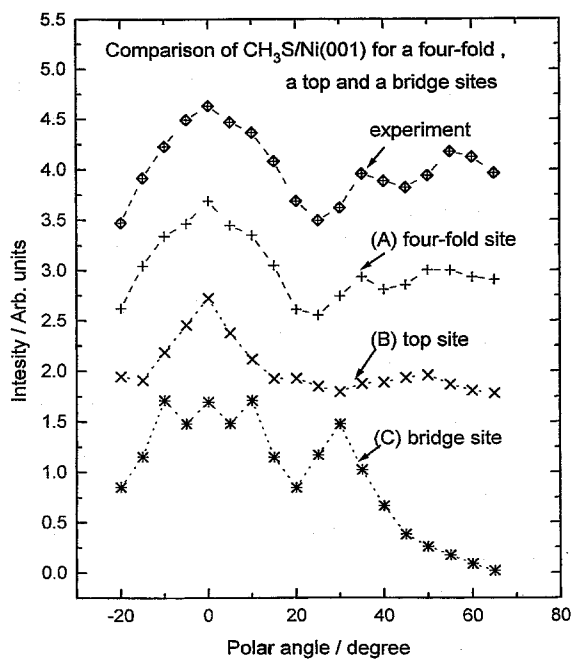

Fig. 7. Comparison of the experimental angular distribution with calculated results for CH_3–S adsorbed at (A) four-fold, (B) atop and (C) bridge sites.

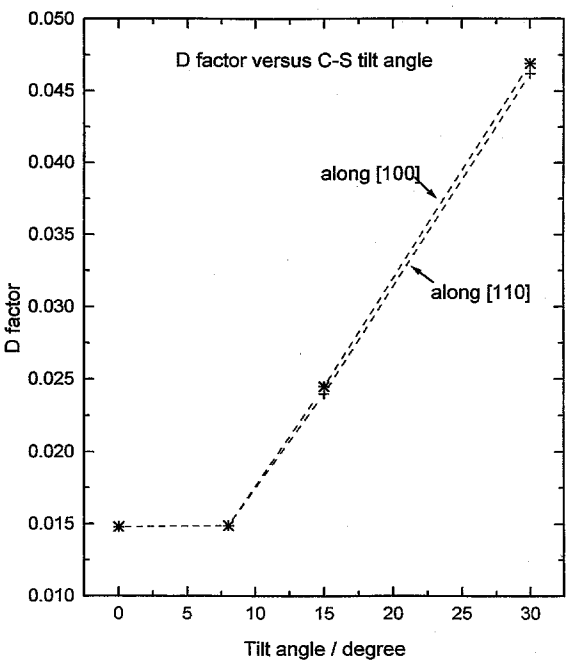

Fig. 8. Plot of the quality of fit parameter D (see text) *versus* the angle of the C–S bond with respect to the surface normal for CH_3S/Ni(001) tilted along the [110] (+) and the [100] (*) azimuths.

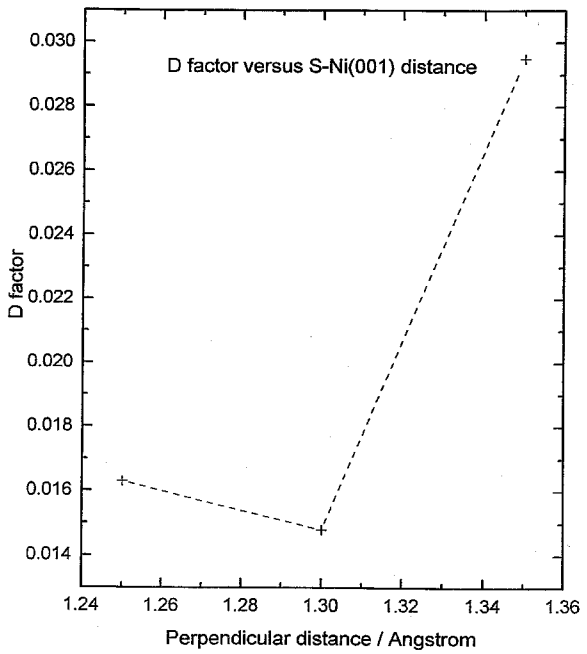

Fig. 9. Plot of the quality of fit parameter D (see text) at the minimum of the graph of D versus C–S bond length (Fig. 10) versus the vertical S–Ni distance for the photoelectron angular distribution of CH_3S/Ni(001).

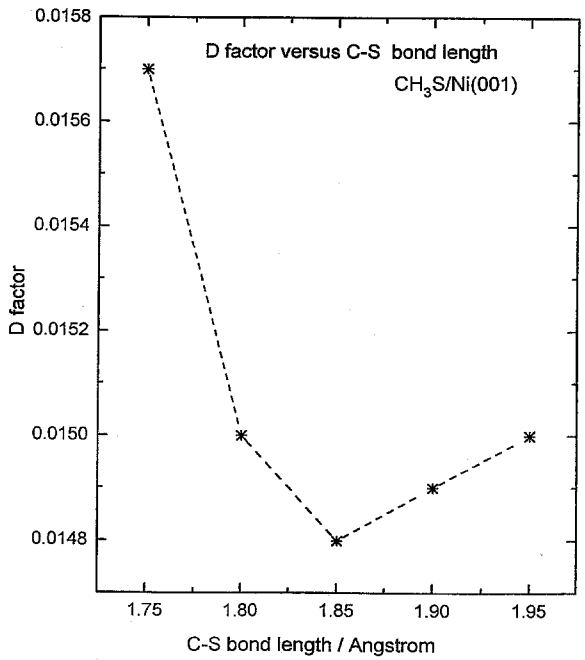

Fig. 10. Plot of the quality of fit parameter D (see text) versus the C–S bond distance for the photoelectron angular distribution of CH_3S/Ni(001).

but indicates that D reaches a minimum for a C–S bond length of 1.85 ± 0.1 Å. The large error in this value reflects the small variation in D as the C–S bond length changes from its minimum value of 1.85 Å. The corresponding value in gas-phase methanethiol is 1.82 Å [23]. The best-fit spectrum calculated for a thiolate adsorbed in a four-fold hollow site with the C–S axis oriented perpendicularly to the surface with a C–S bond length of 1.85 Å and a S–Ni distance of 2.20 Å is shown in Fig. 5.

An advantage of this method is that the data can initially be analyzed rather simply using the notion that outgoing electrons are limited to forward- and back-scattering by atoms located along the axis defined by the emitting atom and the detector. This enables us to limit the number of trial structures that are calculated and compared to the data. This was illustrated in the example given above on methyl thiolate adsorbed on Ni(001), where the approximate sulfur geometry could be determined by comparison with atomic sulfur. The enhanced emission near 0° gave an indication of the C–S bond orientation. Since this idea is only an approximation, final confirmation comes from a comparison of the experimental results with those of a calculation for the electron angular distribution. The excellent agreement between the experimental data and the results of the calculation for a very plausible model suggests that the calculation of the angular distribution can adequately describe this experiment and offers a powerful tool for establishing the nature of adsorbed species on chemically heterogeneous surfaces. A clear drawback of the method is that it requires the correct "guess" of the structure to have been included in the trial models that are tested. Future developments, in which the angular variation of electron photoemitted from the surface is treated as a hologram, offer the possibility of obtaining an initial, perhaps "low-resolution", image of the surface which can then be used as an input into more accurate calculations to establish accurate geometries. This, coupled with the possibility of being able to distinguish different species

from their chemical shifts, renders this a potentially extremely powerful tool.

6. Conclusions

The core-level sulfur 2p photoelectron diffraction pattern from atomic S on Ni(001) is consistent with S adsorbed in the four-fold hollow site. This is confirmed using calculations of the electron angular distribution where the surface is modeled by a sulfur atom adsorbed on a Ni(001) surface where the angular distribution of photoemitted electrons is calculated using a model where the surface is described by a concentric shell of atoms. This yields a result which is in very good agreement with experiment.

A similar strategy reveals that methyl thiolate adsorbs on Ni(001) in the four-fold hollow site with the C–S axis oriented perpendicularly to the surface with a bond length of 1.85 ± 0.1 Å, in good agreement with the corresponding gas-phase value of 1.82 Å. These results indicate that measurement of the angular distribution of photoelectrons provides a method for establishing the nature of adsorbed species on metal surfaces and, when combined with the fact that this angular distribution can be measured for species that have different chemical shifts, potentially provides an extremely powerful method of verifying the nature of species on chemically heterogeneous surfaces.

Acknowledgements

We gratefully acknowledge support of this work by the Division of Chemical Sciences, Office of Basic Energy Sciences, US Department of Energy at Oak Ridge National Laboratory, managed by Lockheed Martin Energy Research Corp. under contract number DE-AC05-96OR22464 (DRM) and the Division of Chemical Sciences, Office of Basic Energy Sciences, US Department of Energy under contract DE-FG02-92ER14289 (WTT), the National Science Foundation (Grant No. DMR-93200275) and the Petroleum Research Fund, administered by the American Chemical Society (D.K.S.). The National Synchrotron Light Source at Brookhaven National Laboratory is supported by the Division of Chemical Sciences and Division of Material Sciences of the US Department of Energy under contract DE-AC02-76CH00016.

References

[1] M.E. Castro and J.M. White, Surf. Sci. 257 (1991) 22.
[2] D.R. Huntley, J. Phys. Chem. 93 (1989) 6156.
[3] M.E. Castro, S. Ahkter, A. Golchet, J.M. White and T. Sahin, Langmuir 7 (1991) 126.
[4] M.R. Albert, J.P. Lu, S.L. Bernasek, D.D. Cameron and J.L. Gland, Surf. Sci. 206 (1988) 348.
[5] B.C. Wiegand, P. Uvdal and C.M. Friend, Surf. Sci. 279 (1992) 105.
[6] J.B. Benziger and R.E. Preston, J. Phys. Chem. 89 (1985) 5002.
[7] D.R. Mullins and P.F. Lyman, J. Phys. Chem. 97 (1993) 9226.
[8] D.R. Mullins and P.F. Lyman, J. Phys. Chem. 97 (1993) 12008.
[9] T.S. Rufael, D.R. Mullins, J.L. Gland and D.R. Huntley, J. Phys. Chem. 99 (1995) 11472.
[10] D.R. Mullins and P.F. Lyman, J. Phys. Chem. 99 (1995) 5548.
[11] D.R. Mullins, P.F. Lyman and S.H. Overbury, Surf. Sci. 277 (1992) 64.
[12] S.H. Overbury, R.J.A. van den Oetelaar and D.R. Mullins, Surf. Sci. 317 (1994) 341.
[13] D.R. Mullins, D.R. Huntley and S.H. Overbury, Surf. Sci. 323 (1995) L287.
[14] D.K. Saldin, G.R. Harp and X. Chen, Phys. Rev. B 48 (1993) 8234.
[15] P.J. Durham, J.B. Pendry and C.H. Hodges, Comput. Phys. Commun. 29 (1982) 193.
[16] D.D. Vvedensky, D.K. Saldin and J.B. Pendry, Comput. Phys. Commun 40 (1986) 421.
[17] C.S. Fadley, in: Synchrotron Radiation Research: Advances in Surface Science, Ed. R.Z. Bachrach (Plenum, New York, 1990).
[18] A. Fernández, J.P. Espinos, A.R. González-Elipe, M. Kerkar, P. Thompson, J. Lüdecke, G. Scragg, A.V. de Carvalho, D.P. Woodruff, M. Fernádez-Garcia and J.C. Conesa, J. Phys.: Condens. Matter 40 (1995) 7781.
[19] Th. Fauster, H. Dürr and D. Hartwig, Surf. Sci. 178 (1986) 657.
[20] J.E. Demuth, D.W. Jepsen and P.M. Marcus, Phys. Rev. Lett. 32 (1974) 1182.
[21] Y. Kitajima, T. Yokoyama, T. Ohta, M. Funabashi, N. Kosugi and H. Kuroda, Surf. Sci. 214 (1989) L261.
[22] Y.-S. Ku and S.H. Overbury, Surf. Sci. 276 (1992) 262.
[23] T. Kojima, J. Phys. Soc. Jpn. 15 (1960) 1284.